ELSEVIER

Chemical Engineering Journal 138 (2008) 349–357

Chemical Engineering Journal

www.elsevier.com/locate/cej

CFD modeling of all gas–liquid and vapor–liquid flow regimes predicted by the Baker chart

Sandra C.K. De Schepper, Geraldine J. Heynderickx *, Guy B. Marin

Laboratorium voor Petrochemische Techniek, Ghent University, Krijgslaan 281 (S5), B-9000 Ghent, Belgium

Received 11 October 2006; received in revised form 31 May 2007; accepted 4 June 2007

Abstract

Calculated gas/vapor–liquid two-phase co-current horizontal flow regimes are compared with experimental data, taken from the Baker chart. For the calculation of the two-phase flow regimes, use is made of the well-known volume of fluid (VOF) multiphase flow model that uses a piecewise linear interface calculation (PLIC) interface reconstruction method in each computational cell, implemented in a computational fluid dynamics (CFD) code.

The flow regimes for water–air flow are reproduced. All simulations give good agreement with the flow regimes expected from the Baker chart. Horizontal flow regimes for two-phase liquid–vapor gasoil flow are also reproduced. To the best of our knowledge, this is the first time that the flow regimes for gasoil liquid–vapor flow as predicted by the Baker chart are simulated. Again, a good agreement between the simulated and expected flow regime is obtained. All horizontal flow regimes appearing in the Baker chart can thus be calculated using CFD.

Keywords: Two-phase flow; Numerical simulation; VOF; PLIC; Baker chart; CFD

1. Introduction

Two-phase gas–liquid or vapor–liquid flows are encountered over a wide range of industrial applications. Due to their complex nature, these flows have mostly been investigated only experimentally. Based on the experimental results, empirical correlations describing the flow, most of them only valid in a limited range of operating conditions, have been developed. However, the growing computer facilities provide the flexibility to construct and use large-scale computational models to calculate these complex two-phase flow types and thus experimental research is not always needed [1].

One of the major difficulties in the modeling of two-phase gas/vapor–liquid flow is the determination of the geometry of the flow field, which can adopt several configurations commonly referred to as flow patterns or flow regimes [2]. Calculating the distribution of the phases in a tube is to be considered as a part of the solution of a chemical engineering problem as it will influence other aspects like heat and mass transfer, pressure drop, etc. [3,4].

In the present work, calculation results for gas/vapor–liquid two-phase co-current horizontal flow patterns are compared with experimental data. The experimental data are taken from the well-known Baker chart [5].

2. Flow pattern maps

Two-phase gas–liquid flow in horizontal tubes is observed in many industrial applications. One of the major difficulties in the modeling of this type of flow is determining the distribution of the liquid and the gas phase in the flow channel. As significant engineering design values such as heat transfer and pressure drop are closely related to this distribution, the calculation of the two-phase flow pattern by means of computational fluid dynamics (CFD) can be very useful [2]. However, these flow calculations are computationally very demanding. Therefore, flow pattern maps are useful tools to identify the type of flow pattern that exists at given flow conditions without having to perform extensive calculations.

Flow pattern or flow regime maps are the result of flow pattern observation experiments. Such experiments are carried out in set-ups in which a gas (or vapor)–liquid mixture is injected in a tube via flow meters, valves and a mixer. The flow pattern in the tube is observed to locate the flow regime on a map. When a

* Corresponding author. Tel.: +32 92644516; fax: +32 92644999.
E-mail address: geraldine.heynderickx@UGent.be (G.J. Heynderickx).

1385-8947/$ – see front matter © 2007 Elsevier B.V. All rights reserved.
doi:10.1016/j.cej.2007.06.007

Nomenclature

F	external body forces (kg/(m^2 s^2))
g	gravitational acceleration (m/s^2)
G	superficial mass velocity of the gas (kg/(m^2 s))
L	superficial mass velocity of the liquid (kg/(m^2 s))
P	pressure (Pa)
S_k	source term for phase k (net rate of production per unit volume) (kg/(m^3 s))
$S_{\alpha k}$	source term for volume fraction of phase k (s^{-1})
t	time (s)
T	temperature (K)
U	fluid velocity (m/s)
U_k	velocity of phase k (m/s)

Greek symbols

α_k	volume fraction of phase k
λ	dimensionless parameter
μ	viscosity (Pa s)
μ_L	liquid viscosity (Pa s)
μ_W	viscosity of water (Pa s)
π	molecular flux of momentum (kg/(ms^2))
ρ	fluid density (kg/m^3)
ρ_A	density of air (kg/m^3)
ρ_G	gas density (kg/m^3)
ρ_L	liquid density (kg/m^3)
ρ_W	density of water (kg/m^3)
σ	gas–liquid surface tension (N/m)
σ_W	water surface tension (N/m)
ψ	dimensionless parameter

broad velocity region is covered for both phases, the boundaries between the different flow type areas can be drawn [3]. The first researcher to acknowledge the importance of flow patterns for the calculation of pressure drop, heat and mass transfer, etc., in tubes was Baker [5]. He published the earliest flow pattern map

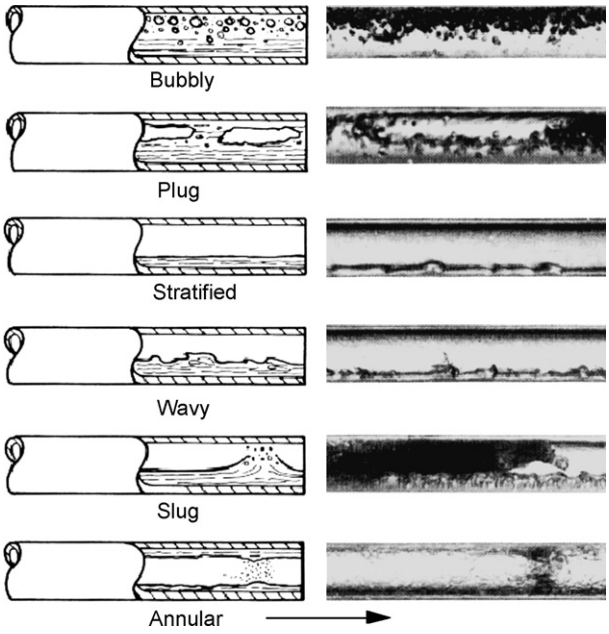

Fig. 2. Horizontal two-phase flow regimes [6].

for horizontal flow in a circular conduit (Fig. 1). Seven different flow regimes were distinguished (Figs. 1 and 2):

- *Stratified flow*: At low liquid and gas velocities, a complete separation of the two phases is observed. The two phases are clearly separated by an undisturbed horizontal interface, with the liquid flowing over the bottom of the tube (under normal gravity conditions).
- *Wavy flow*: When the gas velocity is increased under stratified flow conditions, waves are formed on the liquid–gas interface. These waves travel in the direction of the flow. The amplitude of the waves depends on the relative velocity between the phases and the properties of the fluids, such as their density and surface tension.

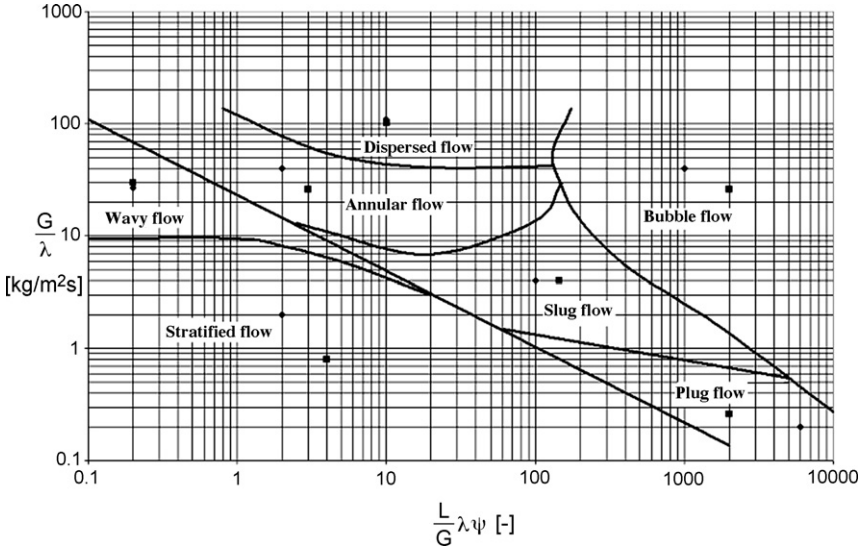

Fig. 1. Baker chart. (●) Operating conditions for the simulations of water–air flow; (■) Operating conditions for the simulations of gasoil liquid–vapor flow

- *Plug flow*: This flow pattern is an intermittent flow that occurs at low gas flow rates and moderate liquid rates. In this regime, liquid plugs, free of entrained gas bubbles, are separated by zones of elongated gas bubbles. The diameters of the elongated bubbles are smaller than the tube diameter. As a result, there is a continuous liquid phase along the bottom of the tube below the elongated bubbles. Plug flow is also referred to as elongated bubble flow.
- *Slug flow*: When the gas velocity is increased under plug flow conditions, the liquid slugs become aerated and contain small gas bubbles. The flow becomes more chaotic as compared to plug flow and the interface between the liquid slugs and the elongated gas bubbles becomes less sharp.
- *Annular flow*: Higher gas flow rates will cause the liquid to form a continuous film around the perimeter of the tube. The film at the bottom of the tube may be much thicker than the film at the top (the thickness variation depends on the velocity of the gas). The interface between the liquid annulus and the gas core is disturbed by small amplitude waves. Liquid droplets can possibly be dispersed in the gas core.
- *Bubble flow*: Gas bubbles are dispersed in the continuous liquid flow.
- *Spray or dispersed flow*: Discrete liquid droplets are dispersed in the continuous gas phase.

The Baker flow regime map (Fig. 1) shows the boundaries of the various flow pattern regions as functions of G, the superficial mass velocity of the gas/vapor phase and L/G, the ratio of superficial mass velocities of the liquid and gas/vapor phase. The dimensionless parameters λ and ψ were added so that the chart could be used for any gas/vapor–liquid combination different from the standard combination. The standard combination, at which both parameters λ and ψ equal unity, is water (W) and air (A) flow under atmospheric pressure and at room temperature. By taking into account appropriate values for λ and ψ, the geometry of two-phase flows with any gas/vapor (G) and any liquid (L) at other pressures and temperatures can be predicted using the same chart.

Although the transition from one flow pattern region to another is presented as a line, in reality these lines are rather broad transition zones. Each researcher probably observed the transition at slightly different superficial flow combinations during the experimental work.

In this work, the seven flow regimes for water/air two-phase flow will be reproduced using a computational fluid dynamics (CFD) two-phase flow model [7,8]. Next, the same model will be used to reproduce the seven flow regimes predicted by the Baker chart for two-phase vapor–liquid gasoil flow, using the appropriate values for the dimensionless parameters λ and ψ (Eqs. (5) and (6)).

3. Multiphase flow modeling

As mentioned before, multiphase flow processes may exhibit several different flow regimes depending on the operating conditions. In general, three steps need to be considered when modeling multiphase flow. A judicious definition of the number of phases next to the consideration of the possible flow regimes and the required resolution are the first crucial steps in selecting the modeling approach. The second step involves the formulation of the governing equations which describe the multiphase flow. Numerical simulation of any flow problem is based on solving the basic flow equations describing the conservation of mass, momentum and energy in the control volume. Finally, the last step in modeling the multiphase flow consists of the solution of these governing equations.

For the calculation of two-phase flow patterns in horizontal tubes in the presented work, use is made of an existing CFD code. This CFD software package is based on the finite volume approach [7]. For the simulations, an Eulerian–Eulerian approach is chosen, in which the grid is fixed and the fluids are assumed to behave as continuous media. From the available Eulerian–Eulerian models in the CFD code, the volume of fluid (VOF) model is chosen [8]. It must however be stressed that if one wants to study a specific flow regime in more detail, the use of other, more appropriate multiphase models must be considered. In the VOF model, used in this work, an Eulerian framework is taken for both phases, combined with a reformulation of interface forces on a volumetric basis [8], as will be explained next.

3.1. VOF model: general description

In the volume of fluid (VOF) model, a single set of conservation equations is shared by the phases and the volume fraction of each of the phases is tracked in each computational cell throughout the domain [8]. These conservation equations can be solved using the appropriate jump boundary conditions at the interface. However, the interface between the different phases does not necessarily remain stationary. As a result, imposing boundary conditions at an interface becomes a very complicated moving boundary problem. To avoid this problem, the VOF model directly determines the motion of all phases and deduces the motion of the interfaces indirectly from this result. Direct tracking of the motion and the deformation of the phase interfaces is thus avoided. All the interfacial forces, therefore, have to be replaced by smoothly varying volumetric forces. If one is in particular interested in the geometry of the interface and the flow patterns near the interface, the VOF model is an interesting model to use. Some interface-related forces, such as surface or adhesion forces, can also be modeled accurately using this modeling approach.

For each additional phase that is added to the model, a variable is introduced: the volume fraction of the phase in the computational cell. In each control volume, the volume fractions of all phases sum up to unity. All control volumes must be filled with either a single fluid phase or a combination of phases. The VOF model does not allow for void regions where no fluid of any type is present. The values for all variables and properties are shared by the phases and calculated as volume-averaged values, as long as the volume fraction of each of the phases is known at a given location. Thus, the variables and properties in any given cell are either purely representative of one of the phases,

or representative of a mixture of the phases, determined by the volume fraction contributions.

In other words, if the kth fluid's volume fraction in the cell is denoted as α_k, then the following three conditions are possible:

- $\alpha_k = 0$: the cell does not contain the kth fluid;
- $\alpha_k = 1$: the cell is full of the kth fluid;
- $0 < \alpha_k < 1$: the cell contains the interface between the kth fluid and one or more other fluids.

Based on the local value of α_k, the appropriate properties and variables will be assigned to each control volume within the domain.

3.2. Governing equations

In the VOF approach, the participating fluids share a single set of conservation equations. The governing equations [8] can, therefore be written:

$$\text{conservation of mass}: \quad \frac{\partial}{\partial t}(\rho) + \nabla \cdot (\rho U) = \sum_k S_k \tag{1}$$

$$\text{conservation of momentum}: \quad \frac{\partial}{\partial t}(\rho U) + \nabla \cdot (\rho U U) = -\nabla \cdot \pi + \rho g + F \tag{2}$$

A physical interpretation can be given to the various terms in the mass conservation equation. The first term of the left-hand side of the mass conservation equation represents accumulation; the second term represents the contribution of convection. The term on the right-hand side represents the sum of volumetric sources of all the fluids. As only flow is considered here, this contribution equals zero.

The physical interpretation of the various terms appearing in the momentum conservation equation follows similar lines. The first term on the left-hand side is the rate of increase in momentum per unit volume; the second term represents the change in momentum per unit volume, caused by convection. The first term on the right-hand side represents molecular contributions, which include pressure and viscous force per unit volume. The last two terms on the right-hand side represent the gravitational force per unit volume and any other external force.

It is straightforward to apply such conservation equations to single-phase flows. In the case of multiphase flows, it is also possible to apply these equations, however, with the appropriate boundary conditions at the interface between the different phases. In particular, density, viscosity and all the other relevant properties will have to change abruptly at the location of the interface. The corresponding methods, which describe and track the time-dependent behavior of the interface itself, are called front tracking methods [9]. The numerical solution of the set of Eqs. (1) and (2) for multiphase flows is extremely difficult and computationally intensive. The main difficulty arises from the interaction between the moving interface and the fixed Eulerian grid that is employed to solve the flow field.

As already explained, the VOF approach simulates the motion of the phases rather than tracking the motion of the interface itself. The motion of the interface is deduced indirectly from the motion of different phases separated by an interface. Motion of the different phases is tracked by solving a continuity equation for a marker function or for the volume fraction of each phase. Thus, when a control volume is not entirely occupied by one phase, mixture properties are used while solving Eqs. (1) and (2). This approach avoids abrupt changes in properties across a very thin interface. The properties appearing in Eqs. (1) and (2) are related to the volume fraction of all phases as follows:

$$\rho = \sum \alpha_k \rho_k, \qquad \mu = \frac{\sum \alpha_k \rho_k \mu_k}{\sum \alpha_k \rho_k} \tag{3}$$

The volume fraction of each fluid α_k, is calculated by tracking the interface between different phases throughout the solution domain. Tracking of the interfaces between N different phases present in the system is accomplished by solving continuity equations of the phase volume fraction for $N-1$ phases. For the kth phase, this equation has the following form:

$$\frac{\partial \alpha_k}{\partial t} + (U_k \cdot \nabla)\alpha_k = S_{\alpha_k} \tag{4}$$

A physical interpretation can be given to the various terms in this continuity equation. The first term of the left-hand side represents accumulation; the second term represents the contribution of convection. The term on the right-hand side represents the sum of volumetric sources of the volume fraction. As only flow is considered here, this contribution equals zero.

By solving this continuity equation for $N-1$ phases, the value of the volume fraction of all phases is determined throughout the solution domain. It must, however, be noted that the phase volume fraction values do not uniquely identify the interface. Different interface configurations may correspond to the same values of these volume fractions. Several specialized techniques have been proposed to track the geometry of the interface accurately. They are described in the next section.

3.3. Interpolation near the interface

In general, a VOF algorithm [9] solves the problem of updating the phase volume fraction field given the fixed grid, the velocity field and the phase volume fraction field as determined in the previous time step. In a two-dimensional problem, the interface is considered to be a continuous, piecewise smooth line. The problem is reduced to the reconstruction of an approximation of the interface in each cell, knowing only the volume fraction of each phase in the cell itself and in the neighboring cells.

The simplest VOF interface tracking methods are the simple line interface calculation (SLIC) algorithms [10]. They are first order in the accuracy for the reconstruction of the interface. Typically, the reconstructed interface is made up of a sequence of segments aligned with the grid, which makes the reconstruction relatively rough. Fig. 3c illustrates the interface reconstruction by means of a SLIC algorithm.

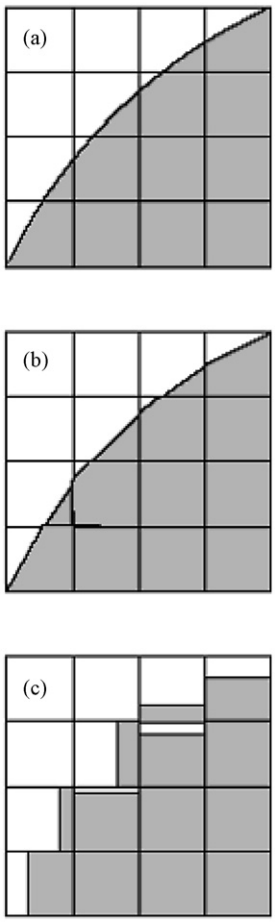

Fig. 3. VOF interface reconstruction methods: (a) actual interface shape, (b) interface reconstruction by means of the second-order or PLIC method, and (c) interface reconstruction by means of the first-order or SLIC method [11].

More accurate VOF techniques attempt to fit the interface through piecewise linear segments. These techniques are known as the piecewise linear interface calculation (PLIC) algorithms [12]. In the PLIC approach, an interface within a computational cell is approximated by a straight line segment with a slope determined from the interface normal. The line segment cuts the computational cell such that the fractional fluid volume equals the value of the phase volume fraction in that cell. The resulting fluid polygon is then used to determine fluxes through any cell face. Fig. 3b illustrates the interface reconstruction by means of a second-order or PLIC algorithm. One of the critical simplifying features of VOF/PLIC algorithms is that it does not attempt to reconstruct the interface as a continuous chain of segments. A discontinuous chain with however small discontinuities is retained. Whenever the curvature is small, the method will be accurate.

A VOF/PLIC algorithm consists of two steps: a reconstruction step and a propagation step. In the reconstruction step, a linear interface that divides the computational cell into two parts containing the proper area of each of the two phases is constructed. The orientation of the segment is determined through the calculation of the unit normal vector to the segment. Several algorithms have been developed for the calculation of the unit normal vector [13]. This unit normal vector, together with the phase volume fraction value in the cell, uniquely determines the linear interface in the cell. The second step of the VOF algorithm is propagation [14]. Once the interface has been constructed, its motion caused by the velocity field must be modeled by a suitable advection algorithm.

During all simulations in the presented work, a PLIC interface reconstruction method has been used for interpolation in a cell. In the existing CFD code, this scheme is the most accurate one and it is applicable for general unstructured meshes as used here. As typical for the PLIC method, this interpolation scheme assumes that the interface between two fluids has a linear slope within each cell and this linear shape is used for the calculation of the advection of the fluid through the cell interfaces. The first step in this reconstruction scheme consists of the calculation of the position of the linear interface relative to the center of each partially filled cell, based on information concerning the volume fraction and its derivatives in the cell. The second step is the calculation of the advecting amount of fluid through each interface using the computed linear interface representation and information about the normal and tangential velocity distribution at the interface. In the third step, the volume fraction in each cell is determined using the balance of fluid mass fluxes calculated in the previous time step.

4. Simulations

4.1. Tube geometry and operating conditions

The simulations are carried out in a horizontal tube with a diameter of 0.08 m and a length of 7 m. The 3D-computational domain was divided into 549,929 hexahedral cells. Near the tube wall, three layers of cells are positioned to assure a correct simulation of the phenomena taking place near the wall.

The VOF model is used for the numerical calculation of the two-phase flow. As mentioned before, this model solves one single set of conservation equations for both phases and tracks the volume fraction of each of the phases throughout the computational domain. In all simulation cases, a PLIC interface reconstruction method is used to track the geometry of the interface accurately.

For all simulations, a no-slip condition is imposed at the tube wall. The influence of the gravitational force on the flow has been taken into account. At the inlet of the tube, uniform profiles for all the variables have been employed. A pressure outlet boundary is imposed to avoid difficulties with backflow at the outlet of the tube.

4.2. Solution strategy and convergence criterion

Because of the dynamic behavior of the two-phase flow, a transient simulation with a time step of 0.001 s is performed. The calculations are performed by combination of the PISO algorithm [15] for pressure–velocity coupling and a second-order upwind calculation scheme [7] for the determination of momentum and volume fraction. The convergence criterion is

Table 1
Operating conditions for the simulations of water–air flow (T = 298 K, P = 101,325 Pa)

	G/λ (kg/(m^2 s))	G (kg/(m^2 s))	$L\lambda\psi/G$	L (kg/(m^2 s))
Stratified flow	2	2	2	4
Wavy flow	27	27	0.2	5.4
Plug flow	0.2	0.2	6000	1200
Slug flow	4	4	100	400
Annular flow	41	41	2	82
Bubble flow	41	41	1000	41,000
Spray flow	109	109	10	1090

based on the residual value of the calculated variables, namely mass, velocity components and volume fraction. In the present calculations, the numerical computation is considered converged when the scaled residuals of the different variables are lowered by four orders of magnitude.

Prior to the two-phase flow calculation (transient simulation), a steady-state simulation is carried out to determine the flow field of one of the phases. Hence, the starting point for the two-phase flow simulations is a fully converged flow field of one phase. Next, both phases are introduced at the inlet and the transient simulation is started. The superficial mass velocities of the liquid and gas/vapor phase, corresponding with a given flow regime according to the Baker chart (Fig. 1), are set as inlet conditions. After a few time steps, the flow of both phases is observed and a given flow regime is established. The phase, initially filling the tube as a result of the steady-state simulation, is pushed out of the tube during the transient simulation.

4.3. Simulation of water–air flow

The first part of the simulation work involves 3D-simulations of the two-phase flow patterns for water and air. For the water–air two-phase system, seven simulation cases under atmospheric pressure and at room temperature have been performed, each one chosen in the center of an operating area representing a different flow regime according to the Baker chart. The superficial mass velocities of water and air, determined from the Baker chart, are set as inlet conditions for the calculation. The operating conditions are given in Table 1 and pointed out in Fig. 1. Both water and air enter the horizontal tube perpendicular to its inlet plane. They have an inlet temperature of 298 K. The fluid pressure at the tube inlet is set to 101,325 Pa. The physical properties of water and air can be found in Table 2.

Table 2
Physical properties of liquid gasoil, gasoil vapor, water and air (T = 298 K, P = 101,325 Pa)

	ρ (kg/m^3)	μ (Pa s)	σ (N/m)
Gasoil liquid	830	0.00332	0.0190355
Gasoil vapor	9.4		
Water	998.2	0.001003	0.0719404
Air	1.225		

Table 3
Operating conditions for the simulations of gasoil liquid–vapor flow (T = 298 K, P = 101,325 Pa)

	G/λ (kg/(m^2 s))	G (kg/(m^2 s))	$L\lambda\psi/G$	L (kg/(m^2 s))
Stratified flow	0.8	2.06	4	0.51
Wavy flow	27	68.63	0.2	0.85
Plug flow	0.3	0.69	2000	85.17
Slug flow	4	10.29	150	95.81
Annular flow	27	68.63	3	12.78
Bubble flow	27	68.63	2000	8516.86
Spray flow	109	274.50	10	170.34

4.4. Simulation of liquid–vapor gasoil flow

The second part of the simulation work involves 3D-simulations of the horizontal flow regimes observed in two-phase liquid–vapor gasoil flow. This set of simulation cases will allow for the first time, to the best of our knowledge, to evaluate the performance of the Baker chart parameters λ and ψ. In all simulation cases, the two-phase flow of gasoil under atmospheric pressure and at room temperature is calculated. The superficial mass velocity of the liquid and vapor phase, corresponding with a given flow regime according to the Baker chart, are set as inlet conditions. Based on the physical properties of liquid gasoil, gasoil vapor, water and air (Table 2), the parameters λ and ψ are calculated:

$$\lambda = \left[\left(\frac{\rho_G}{\rho_A}\right)\left(\frac{\rho_L}{\rho_W}\right)\right]^{0.5} = \left[\left(\frac{9.4}{1.225}\right)\left(\frac{830}{998.2}\right)\right]^{0.5} = 2.53 \quad (5)$$

$$\psi = \frac{\sigma_W}{\sigma}\left[\left(\frac{\mu_L}{\mu_W}\right)\left(\frac{\rho_W}{\rho_L}\right)^2\right]^{1/3} = \frac{0.0719404}{0.0190355}\left[\left(\frac{0.00332}{0.001003}\right)\left(\frac{998.2}{830}\right)^2\right]^{1/3} = 6.37 \quad (6)$$

The resulting operating conditions are given in Table 3 and pointed out in Fig. 1. Both liquid gasoil and gasoil vapor enter the horizontal tube perpendicular to its inlet plane. They have an inlet temperature of 298 K. The pressure at the tube inlet is set to 101,325 Pa. The physical properties of the liquid gasoil and of the gasoil vapor can be found in Table 2. These components and their corresponding physical properties are defined in the materials database of the CFD code.

5. Simulation results

5.1. Water–air flow

The simulation results for the different horizontal flow regimes can be found in Figs. 4 and 5. The figures represent the calculated contours of mixture density (kg/m^3) for the different flow regimes. Since the mixture density is proportional

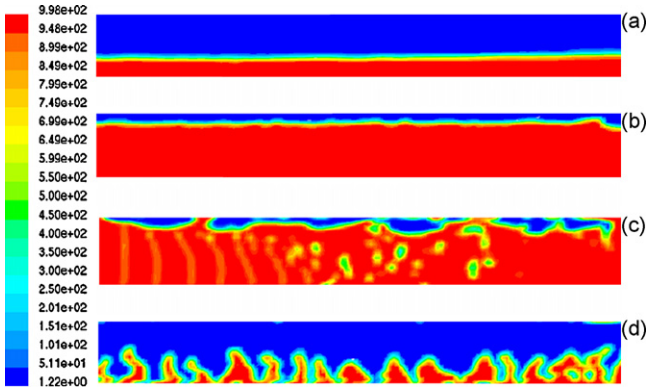

Fig. 4. Contours of mixture density (kg/m^3) for water–air flow: (a) stratified flow, (b) wavy flow, (c) plug flow, and (d) slug flow (operating conditions: see Table 1).

to its phase composition, the distribution of air and water in the tube can be clearly seen. The red color (998 kg/m^3) refers to the presence of pure water, while the dark blue color (1.22 kg/m^3) refers to the presence of pure air.

Fig. 4a shows the simulation results for the operating conditions corresponding with a *stratified* flow regime according to the Baker chart (see Fig. 1 and Table 1). At low liquid and gas velocities and under normal gravity conditions, a flow condition is calculated in which the heavy liquid flows over the bottom of the tube and the gas flows over the liquid. Both phases are separated by a smooth liquid–gas interface.

The simulation results for the *wavy* flow conditions according to the Baker chart (Fig. 1 and Table 1) can be seen in Fig. 4b. Wavy flow is similar to stratified flow but the gas moves at a higher velocity and the interface is disturbed by waves travelling in the direction of the flow. On the figure, the presence of these waves can be clearly seen. Two forces, acting on the wave crest in opposite directions, can be identified. Gravity is the force that tends to flatten the wave and thereby to stabilize the stratified configuration. On the other hand, the Bernoulli force, resulting from the increased air velocity above the wave and the decrease of the pressure in the narrow air gap, tends to increase the wave amplitude. The Bernoulli force and thus the amplitude of the waves is determined by the relative velocity between the phases and the properties of both phases, such as their density and surface tension. Only when the Bernoulli force is larger than the gravitational force, the wavy flow regime appears. In the opposite case, the stratified flow regime will be recognized.

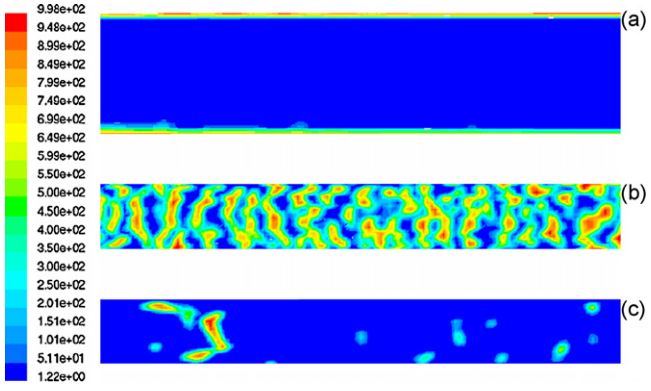

Fig. 5. Contours of mixture density (kg/m^3) for water–air flow: (a) annular flow, (b) bubble flow, and (c) dispersed flow (operating conditions: see Table 1).

Fig. 4c shows the simulation results for a *plug* flow combination according to the Baker chart (see Fig. 1 and Table 1). The plug flow pattern is an intermittent flow regime that occurs at low gas flow rates and moderate liquid flow rates. In this regime, elongated bubbles appear at the top of the tube. In horizontal tubes, due to buoyancy forces, bubbles tend to rise and concentrate at the upper part of the tube and agglomerate to large elongated bubbles. This way, the plug flow regime arises.

The simulation results for the *slug* flow conditions according to the Baker chart (see Fig. 1 and Table 1) are illustrated in Fig. 4d. It can be seen that the slug flow pattern is much more chaotic as compared to the plug flow regime (Fig. 4c). It must however be noticed that the liquid slugs do not touch the upper part of the tube as expected from the observation of Fig. 2. Nevertheless, it can be seen that the calculated flow regime is totally different from the other simulated flow regimes. Although several simulation cases have been carried out to improve the simulation result, Fig. 4d shows the best approximation of the slug flow regime. Remember that the slug flow regime is an intermittent flow regime and the flow pattern region corresponding to slug flow is situated in the middle of the Baker chart (Fig. 1). As mentioned before, broad transition zones between the different flow regimes can be present. Due to these transition zones, it is possible that the region corresponding to the slug flow pattern for water–air flow is very small compared to the other flow pattern regions, which may explain the simulation results, especially the difficulty to simulate a perfect slug flow regime.

Fig. 5a shows the simulation results for the operating conditions corresponding with *annular* flow according to the Baker chart (Fig. 1 and Table 1). The bulk of the liquid forms a film around the inner wall of the pipe and the gas flows at a high velocity through the central core. The annular flow pattern is assumed to exist due to the violent action of the gas stream in dispersing the liquid all around the tube periphery.

The simulation results for the *bubble* flow conditions according to the Baker chart (Fig. 1 and Table 1) can be seen in Fig. 5b. The gas is dispersed as discrete bubbles in the continuous liquid. The bubbles have different shapes and sizes but they are smaller than the tube diameter. The bubble flow regime can be retained by balancing the forces that act on the dispersed bubbles: the buoyancy force which tends to raise the dispersed bubbles to the upper part of the tube and the turbulent force which tends to disperse the bubbles in the pipe.

Fig. 5c shows the simulation results for the *dispersed* flow conditions according to the Baker chart (Fig. 1 and Table 1). In the spray flow regime, small liquid droplets are dispersed in the continuous gas phase.

As can be concluded from the simulation results in the presented figures, all simulations give a good agreement with the expected flow regime. Furthermore, the phenomena, typical for

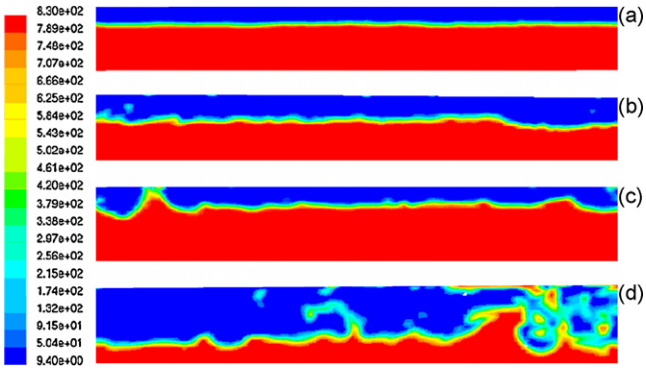

Fig. 6. Contours of mixture density (kg/m^3) for liquid–vapor gasoil flow: (a) stratified flow, (b) wavy flow, (c) plug flow, and (d) slug flow (operating conditions: see Table 3).

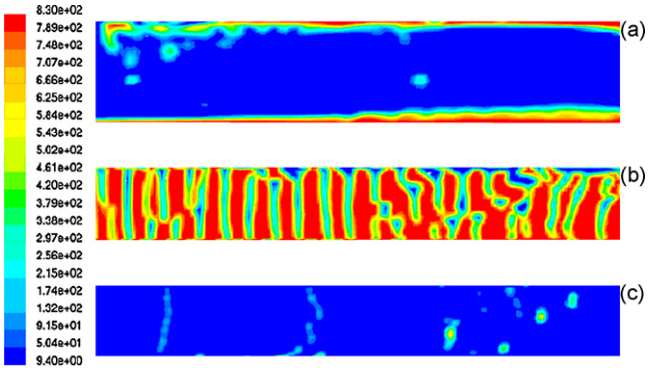

Fig. 7. Contours of mixture density (kg/m^3) for liquid–vapor gasoil flow: (a) annular flow, (b) bubble flow, and (c) dispersed flow (operating conditions: see Table 3).

each flow regime, as described in Section 2, can be distinguished on the figures. For example, in the case of annular flow (Fig. 5a), it can be clearly seen that the liquid film at the bottom of the tube is thicker than the liquid film at the top, due to the gravity forces which are indeed included in the calculations.

Remark that the size of the grid cells determines the magnitude of the phenomena that can be detected with the calculations. Thus, sub-grid scale phenomena cannot be seen on the figures. From the simulation results, it can however be concluded that the constructed mesh is fine enough to be able to simulate all flow regimes. The appearing phenomena are clearly much larger than the sizes of the grid cells. Study of the constructed mesh shows that the smallest features, that are still visible, are of the order of 1 mm. So, only in case of spray flow, it is possible that some liquid droplets, smaller than 1mm, are not visible in the simulation results. However, since it is not our intention to simulate spray flow in detail (in that case an Eulerian–Lagrangian approach should be used) and since the spray flow regime can be clearly recognized in Fig. 5c, it can be concluded that the applied model in combination with the constructed grid is able to simulate all horizontal two-phase flow regimes.

The simulation results have thus shown that the applied CFD models are capable of reproducing the different horizontal two-phase flow regimes. Especially the application of the PLIC interface reconstruction method is a key-factor in the modeling process since this method is known as an accurate and robust method for the determination of the location and geometry of the interface.

5.2. Liquid–vapor gasoil flow

The simulation results for the different horizontal flow regimes can be found in Figs. 6 and 7. The figures represent the calculated contours of mixture density (kg/m^3) for the different flow regimes. Since the mixture density is proportional to its phase composition, the distribution of gasoil vapor and liquid gasoil in the tube can be clearly seen. The red color (830 kg/m^3) refers to the presence of liquid gasoil, while the dark blue color (9.4 kg/m^3) refers to the presence of gasoil vapor.

Fig. 6a shows the simulation results for the operating conditions corresponding with *stratified* flow according to the Baker chart (see Fig. 1 and Table 3). At low liquid and vapor velocities and under normal gravity conditions, the heavier liquid flows over the bottom of the tube, whereas the vapor flows over the liquid. No waves on the liquid–vapor interface can be distinguished.

The simulation results for the *wavy* flow conditions (Fig. 1 and Table 3) can be seen in Fig. 6b. For wavy flow, the vapor phase interacts with the liquid phase, causing surface waves. In the figure, the presence of these waves on the liquid surface can be clearly seen.

Fig. 6c shows the simulation results for the *plug* flow conditions according to the Baker chart (Fig. 1 and Table 3). The plug flow pattern is an intermittent flow regime that occurs at low vapor flow rates and moderate liquid flow rates. In this regime, alternate plugs of liquid and vapor move along the upper part of the tube.

The simulation results for the operating conditions corresponding with a *slug* flow pattern according to the Baker chart (Fig. 1 and Table 3) are illustrated in Fig. 6d. Under slug flow conditions, a wave is picked up periodically by the more rapidly moving vapor to form a frothy slug which passes through the tube at a much higher velocity than the averaged liquid velocity. It must be stressed that, contrary to the water–air simulation (Fig. 4d), the liquid slugs do touch the upper part of the tube, as expected for a slug flow regime based on observations of Fig. 2.

Fig. 7a shows the simulation results for the operating conditions corresponding with *annular* flow according to the Baker chart (Fig. 1 and Table 3). The bulk of the liquid flows along the wall as a thin film and the vapor phase is a continuous phase in the center of the tube.

The simulation results for *bubble* flow conditions according to the Baker chart (Fig. 1 and Table 3) can be seen in Fig. 7b. Bubbles of vapor move along the tube in the continuous liquid flow.

Fig. 7c shows the simulation results for *dispersed* flow operating conditions (Fig. 1 and Table 3). In the spray flow regime, the liquid phase is entrained as a spray by the vapor flow.

From all figures, it can be concluded that the VOF model in combination with the PLIC interface reconstruction method, implemented in the existing CFD code, predicts the expected

flow regime under the given conditions derived from the Baker chart (Fig. 1 and Table 3). Next to that, it is found that the physical properties' expressions for the dimensionless parameters λ and ψ are adequate for making the transition from water–air flow to gasoil liquid–vapor flow. Thus, the performance of the parameters λ and ψ has been evaluated.

The above-presented simulation results confirm that all flow regimes appearing in the Baker chart can be calculated using CFD for two-phase gasoil liquid–vapor flow.

6. Conclusions

The main goal of the presented work was to confirm that CFD codes are able to calculate the different horizontal two-phase flow regimes as predicted by the Baker chart.

In a first step, all horizontal two-phase flow regimes for water–air flow are considered. All simulations give good agreement with the expected flow regime. The flow calculation results obtained with the VOF multiphase model in combination with the PLIC interface reconstruction method, implemented in the CFD code have thus been validated. Especially the application of the PLIC interface reconstruction method determines the quality of the simulated flow regimes since this method is able to determine the location and geometry of the interface with accuracy.

Next to that, all horizontal two-phase flow regimes have been successfully reproduced for gasoil two-phase vapor–liquid flow, making use of that same CFD code. Based on the simulation results, it is also found that the physical properties' expressions for the dimensionless Baker chart parameters λ and ψ are adequate for making the transition from water–air flow to gasoil liquid–vapor flow. To the best of our knowledge, this is the first time that the performance of these parameters has been evaluated.

It can thus be concluded that all horizontal flow regimes appearing in the Baker chart can be simulated using existing CFD codes.

Next it should be shown that evaporation of a liquid flowing through a horizontal tube can be simulated adequately. This will require accounting for the corresponding mass and energy transfer phenomena and the implementation of the latter in existing CFD codes. In-house developed codes will be used to complete the existing CFD codes.

Acknowledgments

Sandra De Schepper would like to thank SABIC Europe for a research assistantship.

The CFD research in thermal cracking (G.J. Heynderickx) is supported by the Fonds voor Wetenschappelijk Onderzoek-Vlaanderen (FWO-Vlaanderen).

References

[1] I. Lun, R.K. Calay, A.E. Holdo, Modelling two-phase flows using CFD, Appl. Energy 53 (1996) 299–314.
[2] S. Ghorai, K.D.P. Nigam, CFD modeling of flow profiles and interfacial phenomena in two-phase flow in pipes, Chem. Eng. Process. 45 (2006) 55–65.
[3] G. Hetsroni, Flow regimes, pressure drop and void fraction, in: Lecture Given at Short Course: Modeling and Computation of Multiphase Flows. Part 1. Bases, The Swiss Federal Institute of Technology, Zurich, Switzerland, 2003.
[4] J.R. Thome, Wolverine Engineering Data Book III. Wolverine Tube Inc., 2004. Free book at website: http://www.wlv.com/products/databook/db3/DatabookIII.pdf.
[5] O. Baker, Simultaneous flow of oil and gas, Oil Gas J. 53 (1954) 185–195.
[6] G.P. Celata, Flow boiling, in: Lecture Given at Course: Boiling Heat Transfer and Boiling Equipment, CISM, Udine, Italy, 2005.
[7] H.K. Versteeg, W. Malalasekera, An Introduction to Computational Fluid Dynamics, the Finite Volume Method, Longman Scientific and Technical, Harlow, Essex, UK, 1995.
[8] V.V. Ranade, Computational Flow Modeling for Chemical Reactor Engineering, vol. 5, Academic Press, St. Louis, MO, USA, 2002.
[9] S. Zaleski, Interface tracking—VOF, in: Lecture Given at Course: Industrial Two-phase Flow CFD, von Karman Institute for Fluid Dynamics, Belgium, 2005.
[10] W. Noh, P. Woodward, SLIC (simple line interface calculation), in: A. van de Vooren, P. Zandbergen (Eds.), Proceedings of the Fifth International Conference on Fluid Dynamics, vol. 59: Lecture Notes in Physics, Springer, Berlin, 1976, pp. 330–340.
[11] Fluent Inc., Fluent 6.2 User's Guide, Fluent Inc., Lebanon, USA, 2005.
[12] J. Li, Calcul d'interface affiné par morceaux (piecewise linear interface calculation), C.R. Acad. Sci. Paris Série IIb: Paris 320 (1995) 391–396.
[13] E.G. Puckett, A volume-of-fluid interface tracking algorithm with applications to computing shock wave refraction, in: H. Dwyer (Ed.), Proceedings of the Fourth International Symposium on Computational Fluid Dynamics, Davis, CA, 1991, pp. 933–938.
[14] E.G. Puckett, A.S. Almgren, J.B. Bell, D.L. Marcus, W.J. Rider, A high-order projection method for tracking fluid interfaces in variable density incompressible flows, J. Comput. Phys. 130 (1997) 269–282.
[15] R.I. Issa, Solution of the implicitly discretized fluid flow equations by operator splitting, J. Comput. Phys. 62 (1986) 40–65.